第 44 卷 第 9 期/2024 年 5 月/光学学报 研究论文

光学学报

光子自旋解耦合的人工表面等离激元双功能波前调控

杨清秀[1]，席科磊[1]，周韶东[1]，盛小航[1]，张文雅[1,2]，高靖翔[1]，王桂芳[3]，庄松林[1]，程庆庆[1,3*]

[1]上海理工大学光电信息与计算机工程学院，上海 200093；

[2]中国科学院上海光学精密机械研究所微纳光电子功能材料实验室，上海 201800；

[3]温州医科大学附属衢州医院呼吸科，浙江 衢州 324000

摘要 多功能超表面的研究和开发是光子学的研究热点，光子自旋解耦合的实现对多功能超表面的制备至关重要。利用光子自旋霍尔效应将不同手性的圆偏振光分离，已经取得显著的研究成果。然而，其分离后的圆偏振光的几何相位是互为共轭的，无法对两种圆偏振光的相位实现完全独立且自由的调控。本文通过几何相位和共振相位的联合使用，打破了几何相位之间的共轭关系，实现了不同手性圆偏振光的自旋解耦，从而设计出了一款基于人工等离子体极化激元的双功能波前自由调控耦合器。在 75 GHz线偏振光源的激励下，耦合器的左右两侧模拟实现了效率分别为 41% 和 37% 的聚焦光束和贝塞尔光束。本文为多功能元器件的制备和光子集成的片上器件提供了新的设计方案和思路。

关键词 光子自旋霍尔效应；偏振转换；超构表面；高效耦合器；表面波

中图分类号 O436 **文献标志码** A **DOI**：10.3788/AOS231946

1 引 言

超表面是由尺寸为亚波长的单元结构按照一定的功能序在界面上的二维排布[1-2]，在自由空间的多自由度光场调控中充当着重要的载体[3]。经典 Pancharatnam-Berry（PB）相位的超表面，由连续旋转单元结构实现相位控制，不同自旋态光子因受相反相位梯度的调控进而分离，是目前用来操纵手性光束的理想工具。基于此，已经报道了诸多有趣现象，如光子自旋霍尔效应[4-7]、偏振转换光束的高效生成[8-9]和全息[10-12]等。然而，不同手性光子的 PB 相位受共轭关系约束，具有等大且反号的相位关系，这限制了对不同手性偏振光的独立控制。随后，多种自旋解耦合理论被提出，2017 年，Capasso 课题组[13]揭示了 PB 相位叠加传输相位的联合调控途径，实现了任意正交偏振态的独立相位全息生成。引入非手性相位和 PB 相位的结合，能够打破 PB 相位对手性光子施加的共轭关系，多功能器件进而得以快速发展[14-15]。传输相位联合 PB 相位实现自旋解耦合，实现了光束偏转[16-19]、涡旋光束模式切换的独立控制[19-20]、对信道复用[21]等。共振相位联合 PB 相位，实现了表面波和空间波的转换[22-23]、涡旋光束激发[24]、双功能波前调控[25-29]等。手性无关的相位联合 PB 相位为自旋解耦合提供了多种新颖方法，为手性光束的多功能复用提供了可行性。此外，通过优化金属结构来设计表面电流的路径，当不同手性的圆偏振光激发结构的表面电流时，表面电流有不同的旋转角度，即达成了几何相位的自旋解耦。

除了在自由空间中的传播模式，电磁波还存在于束缚的本征模式，即表面等离子体极化激元（SSPP）模式，是由光激发出的金属电子集体振荡与入射光的电磁场紧密耦合，形成的一种沿着金属表面传播的电磁波[31-34]，能够在纳米尺度上局域和操控光场，广泛应用于光电器件（如传感器、传输线等）[35-36]、微量元素检测[37]、光学显微镜[38]、集成电路[39]，以及热载流子动力学[40]等方面。然而，SSPP 的高效激发和波前工程仍然面临巨大挑战，不利于其应用在小型化的集成设备中。最近，用超表面激发 SSPP 模式表面波（SW）为轻量化耦合器的制备提供了思路，如 SW 的高效激发[41]、与手性相关的 SW 定向耦合[42-44]、SW 波前偏转或聚焦[33]等。

本文设计出了共振相位和 PB 相位相结合的自旋解耦合超表面，实现了 SSPP 模式的激发以及双功能波前调控。该结构基于一种偏振转换效率接近 100% 的“工”字形单元结构，结合 PB 相位，实现了将自由空间传播模式电磁波高效地耦合成面内传输的 SSPP 模式。特别地，通过引入共振相位，打破了自旋态之间

收稿日期：2023-12-19；**修回日期**：2024-02-01；**录用日期**：2024-02-23；**网络首发日期**：2024-03-13

基金项目：国家自然科学基金（11874266，12174260）、上海市科学技术委员会启明星项目（21QA1406400）、上海市科学技术委员会面上项目（21ZR1443500，21ZR1443600）

通信作者：*qqcheng@usst.edu.cn

相位的共轭锁定，为双功能波前的设计创造了条件。

2　高效耦合器的设计原理

2.1　高效耦合器的原理性分析

首先考虑超表面中单个单元结构的电磁响应，具有镜面对称性的反射式单元结构的光学特性可以由琼斯矩阵表征为 $\boldsymbol{R}=\begin{pmatrix} r_{uu} & 0 \\ 0 & r_{vv} \end{pmatrix}$，$u$ 和 v 分别为单元结构的两个主轴方向。在单元结构绕 z 轴旋转角度 θ 的情况下，对应的琼斯矩阵表示为

$$\boldsymbol{R}(\theta)=\boldsymbol{M}^{\mathrm{T}}(\theta)\times\boldsymbol{I}\times\boldsymbol{M}(\theta), \tag{1}$$

式中 $\boldsymbol{M}(\theta)=\begin{pmatrix} \cos\theta & \sin\theta \\ -\sin\theta & \cos\theta \end{pmatrix}$ 为旋转矩阵。进一步，以圆极化 $\boldsymbol{e}_{\pm}=\frac{\sqrt{2}}{2}\begin{pmatrix} u \\ \pm \mathrm{i}v \end{pmatrix}$ 为新基矢代入式(1)得

$$\begin{aligned}\boldsymbol{R}(\theta)=&\frac{1}{2}(r_{uu}+r_{vv})\boldsymbol{I}+\frac{\mathrm{i}}{2}(r_{uv}-r_{vu})\boldsymbol{\sigma}_3+\\&\frac{1}{2}(r_{uu}-r_{vv})(\mathrm{e}^{-\mathrm{i}2\theta}\boldsymbol{\sigma}_{+}+\mathrm{e}^{\mathrm{i}2\theta}\boldsymbol{\sigma}_{-})+\\&\frac{\mathrm{i}}{2}(r_{uv}+r_{vu})(-\mathrm{e}^{-\mathrm{i}2\theta}\boldsymbol{\sigma}_{+}+\mathrm{e}^{\mathrm{i}2\theta}\boldsymbol{\sigma}_{-}),\end{aligned} \tag{2}$$

式中：$\boldsymbol{\sigma}_1$、$\boldsymbol{\sigma}_2$、$\boldsymbol{\sigma}_3$ 为 Pauli 矩阵；$\boldsymbol{I}$ 为单位矩阵；$\boldsymbol{\sigma}_{\pm}(\boldsymbol{\sigma}_1\pm\boldsymbol{\sigma}_2)/2$（正负号取决于入射光的手性，入射光为左旋圆偏振光时为正，入射光为右旋圆偏振光时为负）。特别地，对式(2)进行分析得到偏振转换条件为

$$\begin{cases}\boldsymbol{\sigma}_{-}|\boldsymbol{L}\rangle=|\boldsymbol{R}\rangle,\boldsymbol{\sigma}_{+}|\boldsymbol{R}\rangle=|\boldsymbol{L}\rangle \\ \boldsymbol{\sigma}_{+}|\boldsymbol{L}\rangle=\boldsymbol{O},\boldsymbol{\sigma}_{-}|\boldsymbol{R}\rangle=\boldsymbol{O}\end{cases}, \tag{3}$$

式中，$\boldsymbol{O}$ 为零向量。由上述单元结构构成的超表面，在受到特定手性的圆偏振光照射时会产生两束反射光束，即寻常反射光束和偏振转换光束，其分别表现出与入射光相同和相反的手性。寻常光束是入射光束的镜面反射光束，其出射效率仅取决于式(2)前两项的系数。不同于寻常反射光束，偏振转换光束则是由不同单元结构散射波之间的干涉重构而成的光束，其出射效率仅取决于式(2)后两项的系数。在不考虑材料损耗的情况下，根据能量守恒，寻常反射光束强度为 0 时，超表面可实现 100% 的偏振转换效率，即

$$\begin{cases}|r_{uu}+r_{vv}|=0 \\ |r_{uv}-r_{vu}|=0^{\circ}\end{cases} \tag{4}$$

由于镜像对称的结构必然满足 $r_{uv}=r_{vu}=0$，因此，为实现 100% 的偏振转换效率只需要满足 $r_{uu}=-r_{vv}$。在这种情况下，偏振转换光束的反射系数等于 1，即 $\frac{1}{2}(r_{uu}-r_{vv})=1$。为此，单元结构需要满足以下条件：

$$\begin{cases}|r_{uu}|=|r_{vv}|=1 \\ \arg(r_{uu})-\arg(r_{vv})=180^{\circ}\end{cases}^{\circ} \tag{5}$$

式(5)表明，需要设计的结构是一个反射式的完美半波片，即反射式单元结构的同极化率为 1，且同极化反射的相位差为 180°。

2.2　结构设计

基于式(5)所设计的 PB 单元结构的几何结构如图 1(a)所示。单元结构由金属-绝缘体-金属三层结构组成，其中上层为“工”形谐振器以及底层金属为厚度 $t=1\ \mu\mathrm{m}$ 的金膜；环形结构的半径 $r=0.26\ \mathrm{mm}$，圆环的宽度 $w=0.12\ \mathrm{mm}$，开口角 $\alpha=25°$；介质层是厚度为 $h=0.3\ \mathrm{mm}$ 的 FR-4；元胞的周期 $p=1\ \mathrm{mm}$。通过 CST Microwave Studio 2020 对结构进行仿真分析，x 和 y 方向的边界条件设置为 unit cell，z 方向的边界条件设置为 open add (space)。在偏振方向分别为 x 和 y 方向的线偏振光激励下，超表面的同极化率 r_{uu}、r_{vv} 与相应的反射相位 ϕ_{uu}、ϕ_{vv} 如图 1(b)所示。在 75 GHz 时，超表面的反射相位差 $\phi_{uu}-\phi_{vv}=180°$，反射率 $|r_{uu}|=0.96$、$|r_{vv}|=0.92$（近似为 1），符合式(5)对单元结构的要求。接下来，采用圆偏振光作为入射光源，超表面在圆偏振光激励下的偏振转换效率如图 1(c)所示。R_1 为左/右旋圆偏振光到右/左旋圆偏振光之间的偏振转换效率，R_2 是左/右旋圆偏振光到左/右旋圆偏振光之间的寻常反射光束的反射效率。在 75 GHz 时，偏振转换效率 R_1 为 0.92，寻常反射光束的反射效率 R_2 为 0.05。

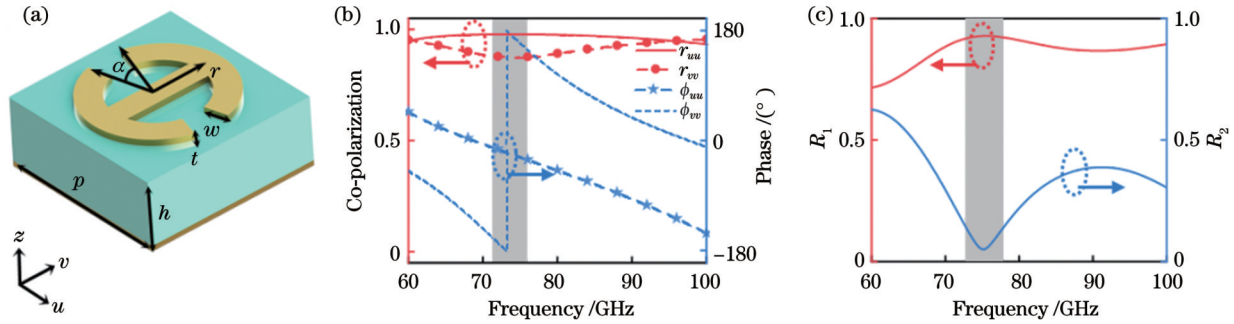

图 1　具有高偏振转换效率的单元结构。(a)单元结构设计图；(b)频率范围为 60～100 GHz 时，使用(a)中的单元结构构建的超表面对线偏振光源的同极化率和对应的反射相位；(c)圆偏振光之间的偏振转换效率

Fig. 1　A unit with high-efficiency polarization conversion capability. (a) Design diagram of unit structure; (b) when frequency range is from 60 to 100 GHz, co-polarization ratio and corresponding reflection phase of a metasurface constructed using unit structure in (a) for inearly polarized light sources; (c) polarization conversion efficiency between circularly polarized lights

3　SSPP模式电磁波的激发

现在利用得到的PB单元结构来设计激发SSPP的耦合器。由于金属在微波频段不支持自然表面等离子体模式的电磁波，首先设计一种支持微波频段SSPP的波导结构。该波导由上下两层组成，下层是厚度为 $t=1\ \mu m$ 的金层，上层是厚度为 $h=0.3\ mm$ 的FR-4介质层，如图2(a)所示。这种波导所支持的SSPP模式的色散图如图2(b)所示。接下来，利用提出的PB单元结构设计一个相位梯度 $\xi=2\theta/p=k_x=1.12k_0$（$\xi>k_0-k_0\sin\theta_i$，$\xi$为相位梯度，$\theta_i$为入射角）的超表面[45]，该相位梯度很好地满足75 GHz时波导上的SSPP模式的波矢匹配条件。将设计的PB单元结构沿 x 方向排布并按照恒定的步长 $\Delta\theta=45^\circ$ 连续旋转，如图2(b)所示。将所设计的波导与超表面组合以构成等离子体激元耦合器，其相位调制结果为

$$\Phi^\sigma(x,y)=\Phi_0+\sigma\xi\cdot x, \tag{6}$$

式中，$\sigma=\pm1$（入射光为左旋圆偏振光时对应着 $\sigma=1$，入射光为右旋圆偏振光时对应着 $\sigma=-1$）。由式(6)可知，入射光束手性不同时，出射波会分别在耦合器的 x 轴上沿相反的方向传播（左旋圆偏振光入射时出射方向在耦合器右侧，右旋圆偏振光入射时出射方向在耦合器左侧）。

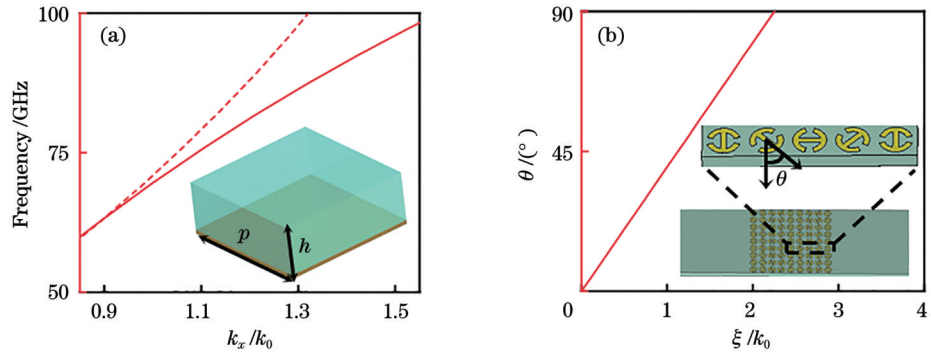

图2　将自由空间电磁波耦合为SSPP模式的表面波的超表面耦合器。(a)耦合器两端平板波导的色散关系；(b)单元结构的转角 θ 与相位梯度的对应关系

Fig. 2　Metasurface coupler that couples free-space electromagnetic waves into surface wave modes as SSPP modes. (a) Dispersion relationship between two end flat waveguides of coupler; (b) correspondence between rotation angle θ of unit structure and phase gradient

为了清晰地呈现本文设计的超表面同时具有SSPP模式电磁波的高效激发以及双功能波前调控的特征，模拟上以线偏振光作为照射光源，在片上的左右两边同时得到了聚焦光束和贝塞尔光束的效果，如图3所示。

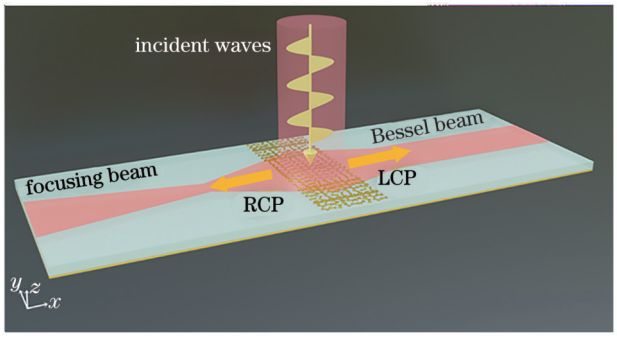

图3　耦合器左侧为线偏振光分解的右旋圆偏振(RCP)光激发的聚焦光束，右侧为线偏振光分解的左旋圆偏振(LCP)光激发的贝塞尔光束

Fig. 3　On left side of coupler is focusing beam excited by right circularly polarization (RCP) light decomposed by linearly polarization light, and on right side is Bessel beam excited by left circularly polarization (LCP) light decomposed by linearly polarization light

4　双功能波前的独立调控

4.1　共振相位

由于不同手性的圆偏振光激发的PB相位是严格相反的，因此上述耦合器左右两侧表面波的波前效果并不是独立的，而是紧密联系在一起的。为实现这两种波前的独立调控，本文设计了一种耦合器件，通过引入与手性无关的相位打破自旋锁定，实现了SSPP模式的激发与双波前独立调控。从式(2)可得到，对于整个反射体系，反射系数为

$$r=\frac{1}{2}(r_{uu}-r_{vv})e^{i\phi_{PB}}=\frac{1}{2}(R_{uu}-R_{vv})e^{i(\phi_{res}+\phi_{PB})}, \tag{7}$$

式中，$\phi_{res}=\arg(r_{uu}-r_{vv})$ 为共振相位，其大小取决于结构本身而不受入射光手性的影响，因此可以通过引入共振相位这一自由度来打破自旋锁定。

通过对单元结构参数进行扫描，观察到单元结构的开口角 α 可以有效调控共振相位。在75 GHz的线偏振入射光激励下，α 与共振相位的关系如图4(a)所示。当 α 从5°增大到140°时，对应的 ϕ_{res} 的调控区间为−90°～90°。分别沿 u 方向和 v 方向的入射线偏振光的同极化率和反射相位与 α 之间的关系如图4(b)所示。在改变 α 的过程中，同极化率 r_{uu} 和 r_{vv} 几乎不发

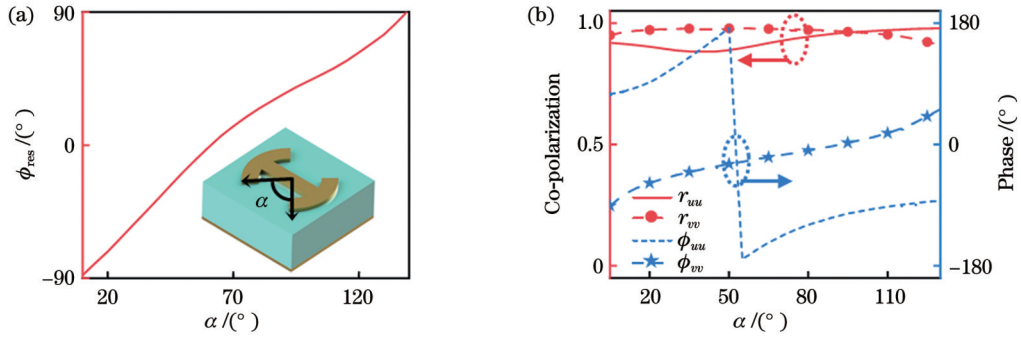

图 4　改变单元结构的开口角 α 值对结构性能的影响。(a)频率为 75 GHz 时，结构的共振相位与 α 的对应关系；(b)频率为 75 GHz 时，开口角 α 对结构反射率及反射相位的影响

Fig. 4　Influence of changing opening angle α value of unit structure on its performance. (a) Correspondence between resonant phase of structure and α when frequency is 75 GHz; (b) influence of opening angle α on structure's reflectance and reflection phase when frequency is 75 GHz

生变化，始终保持在 1 左右。同时，ϕ_{uu} 和 ϕ_{vv} 的差值始终保持在 180°左右，即改变开口角 α 后，单元结构依然具有半波片的特性。因此，调控 α 可以在保证偏振转换效率的前提下打破自旋锁定，实现双功能波前调控。

4.2　双功能波前独立调控耦合器的设计

基于上述理论，可设计一款能够实现双功能波前调控的耦合器件，在不同手性圆偏振光激励下，在耦合器左右两侧分别实现聚焦和贝塞尔表面波。为此，在 x 方向上按照 45°的恒定步长旋转单元结构以实现 SSPP 模式的激发，在 y 方向通过调整开口角度 α 实现波前剪裁，在 y 方向排列结构的开口角度可由图 4(a)检索得到。对应的相位分布为

$$\begin{cases}\phi_{\mathrm{L}}=-\xi\cdot|x|+\xi\cdot|y|\cdot NA=-\phi_{\mathrm{PB}}+\phi_{\mathrm{res}}\\ \phi_{\mathrm{R}}=\xi\cdot|x|-\xi\cdot\left(\sqrt{y^2+f^2}-f\right)=\phi_{\mathrm{PB}}+\phi_{\mathrm{res}}\end{cases},\tag{8}$$

式中：相位梯度 $\xi=1.12k_0$；数值孔径 $NA=0.3$；焦距 $f=13$ mm。

根据式(8)计算的相位分布，在波导结构上排列单元结构，设计的耦合器尺寸为 80 mm×23 mm。在 75 GHz 的线偏振光激励下，$z=1$ mm 处 x-y 平面上的电场(E_z)分布情况如图 5 所示。在耦合器左侧实现聚焦效果，分别采集了 $x=-15.45$、-13.65、-11.85 mm 处场强 E_z 的分布情况，如图 5(a)所示，其半峰全宽分别为 2.21、1.74、2.21 mm，在 $x=-13.65$ mm 处具有最小

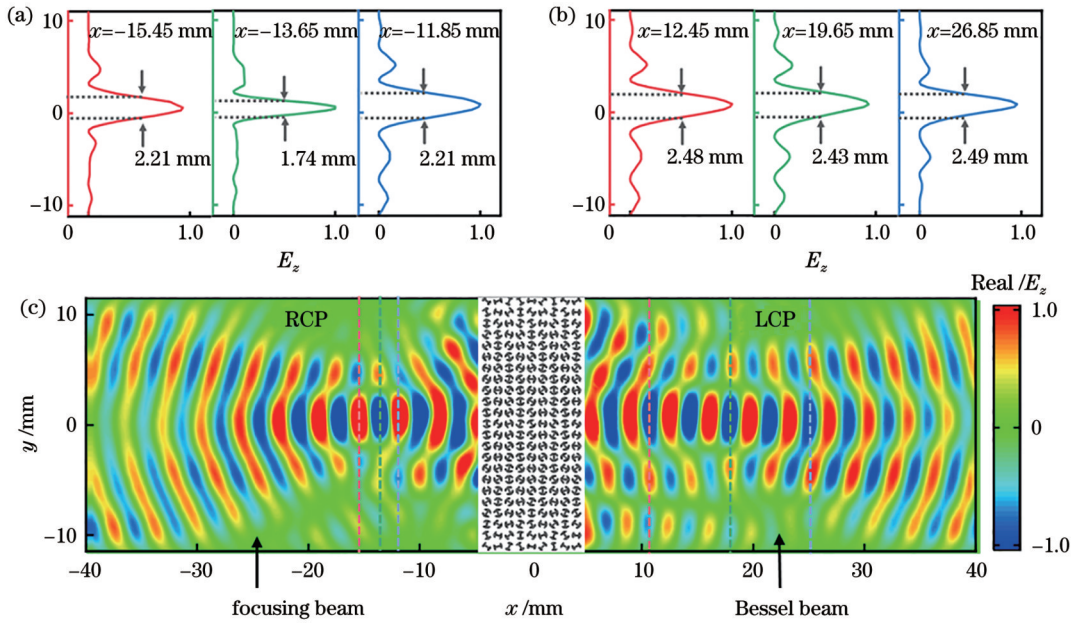

图 5　波前独立调控效果。(a)聚焦光束在 $x=-15.45$、-13.65、-11.85 mm 处的中心场强的半峰全宽；(b)贝塞尔光束在 $x=12.45$、19.65、26.85 mm 处中心场强的半峰全宽；(c)聚焦光束和贝塞尔光束的电场图

Fig. 5　Wavefront-independent control effect. (a) Full width at half wavelength of central field intensity of focusing beam at $x=-15.45$, -13.65, and -11.85 mm; (b) full width at half wavelength of central field intensity of Bessel beam at $x=12.45$, 19.65, and 26.85 mm; (c) electric field patterns of focusing beam and Bessel beam

的半峰全宽。在耦合器右侧实现贝塞尔光束，分别采集了 x=12.45、19.65、26.85 mm 处场强 E_z 的分布情况，如图 5(b)所示，其半峰全宽分别为 2.48、2.43、2.49 mm，无衍射长度为 15 mm。为了进一步表征耦合器的性能，定义耦合效率为出射场功率与入射场功率之比。通过仿真计算左侧聚焦光束与右侧贝塞尔光束的耦合效率分别为 41% 和 37%，与设计目标保持良好的一致性。

5 结　论

本文利用具有高效偏振转换功能的单元结构，设计了一款能激发 SSPP 模式平面波的耦合器，在频率为 75 GHz 的线偏振光激励下，成功地在耦合器两侧通过仿真模拟实现了效率分别为 41% 和 37% 的聚焦光束和贝塞尔光束，模拟结果与设计目标吻合。耦合器的设计利用了共振相位和 PB 相位的双自由度调控，即通过对每个晶胞转角和开口角的精确设置，打破了 PB 相位的共轭锁定，实现了不同手性圆偏振光激励下的波前独立调控。该器件的小尺寸以及多功能的特点有望在未来应用于集成光学领域。

参 考 文 献

[1] Yu N F, Genevet P, Kats M A, et al. Light propagation with phase discontinuities: generalized laws of reflection and refraction [J]. Science, 2011, 334(6054): 333-337.

[2] Degl' Innocenti R. Terahertz metasurface platform for modulation, holography, and encryption[J]. Advanced Photonics, 2023, 5(2): 020503.

[3] Fan Q B, Liu M Z, Zhang C, et al. Independent amplitude control of arbitrary orthogonal states of polarization via dielectric metasurfaces[J]. Physical Review Letters, 2020, 125(26): 267402.

[4] Shitrit N, Bretner I, Gorodetski Y, et al. Optical spin Hall effects in plasmonic chains[J]. Nano Letters, 2011, 11(5): 2038-2042.

[5] Huang L L, Chen X Z, Mühlenbernd H, et al. Dispersionless phase discontinuities for controlling light propagation[J]. Nano Letters, 2012, 12(11): 5750-5755.

[6] Yin X B, Ye Z L, Rho J, et al. Photonic spin Hall effect at metasurfaces[J]. Science, 2013, 339(6126): 1405-1407.

[7] Shitrit N, Yulevich I, Maguid E, et al. Spin-optical metamaterial route to spin-controlled photonics[J]. Science, 2013, 340(6133): 724-726.

[8] Duan J W, Guo H J, Dong S H, et al. High-efficiency chirality-modulated spoof surface plasmon meta-coupler[J]. Scientific Reports, 2017, 7: 1354.

[9] Jia M, Wang Z, Li H T, et al. Efficient manipulations of circularly polarized terahertz waves with transmissive metasurfaces[J]. Light, Science & Applications, 2019, 8: 16.

[10] Chen W T, Yang K Y, Wang C M, et al. High-efficiency broadband meta-hologram with polarization-controlled dual images[J]. Nano Letters, 2014, 14(1): 225-230.

[11] Huang L L, Chen X Z, Mühlenbernd H, et al. Three-dimensional optical holography using a plasmonic metasurface[J]. Nature Communications, 2013, 4: 2808.

[12] Zheng G X, Mühlenbernd H, Kenney M, et al. Metasurface holograms reaching 80% efficiency[J]. Nature Nanotechnology, 2015, 10: 308-312.

[13] Mueller J P B, Rubin N A, Devlin R C, et al. Metasurface polarization optics: independent phase control of arbitrary orthogonal states of polarization[J]. Physical Review Letters, 2017, 118(11): 113901.

[14] Ding G W, Chen K, Luo X Y, et al. Dual-helicity decoupled coding metasurface for independent spin-to-orbital angular momentum conversion[J]. Physical Review Applied, 2019, 11(4): 044043.

[15] Overvig A C, Shrestha S, Malek S C, et al. Dielectric metasurfaces for complete and independent control of the optical amplitude and phase[J]. Light: Science & Applications, 2019, 8(1): 92.

[16] Shalaev M I, Sun J, Tsukernik A, et al. High-efficiency all-dielectric metasurfaces for ultracompact beam manipulation in transmission mode[J]. Nano Letters, 2015, 15(9): 6261-6266.

[17] Li S Q, Wang Z, Dong S H, et al. Helicity-delinked manipulations on surface waves and propagating waves by metasurfaces[J]. Nanophotonics, 2020, 9(10): 200.

[18] Bai G D, Ma Q, Li R Q, et al. Spin-symmetry breaking through metasurface geometric phases[J]. Physical Review Applied, 2019, 12(4): 044042.

[19] Zhang Y P, Jiang C Y, Li Z K, et al. Circularly polarized terahertz wave independently controlled tunable spin-decoupled metasurface[J]. Results in Physics, 2024, 56: 107287.

[20] Li J S, Chen J Z. Simultaneous and independent regulation of circularly polarized terahertz wave based on metasurface[J]. Optics Express, 2022, 30(12): 20298-20310.

[21] Xu P, Liu H X, Li R J, et al. Dual-band spin-decoupled metasurface for generating multiple coaxial OAM beams[J]. IEEE Transactions on Antennas and Propagation, 2022, 70(11): 10678-10690.

[22] Ding F, Deshpande R, Bozhevolnyi S I. Bifunctional gap-plasmon metasurfaces for visible light: polarization-controlled unidirectional surface plasmon excitation and beam steering at normal incidence[J]. Light: Science & Applications, 2018, 7(4): 17178.

[23] Luo W J, Sun S L, Xu H X, et al. Transmissive ultrathin Pancharatnam-Berry metasurfaces with nearly 100% efficiency [J]. Physical Review Applied, 2017, 7(4): 044033.

[24] Dong S H, Li S Q, Ling X H, et al. Broadband spin-unlocked metasurfaces for bifunctional wavefront manipulations[J]. Applied Physics Letters, 2022, 120(18): 181702.

[25] Gou Y, Ma H F, Wu L W, et al. Broadband spin-selective wavefront manipulations based on Pancharatnam-Berry coding metasurfaces[J]. ACS Omega, 2021, 6(44): 30019-30026.

[26] Guo W L, Wang G M, Ji W Y, et al. Broadband spin-decoupled metasurface for dual-circularly polarized reflector antenna design[J]. IEEE Transactions on Antennas and Propagation, 2020, 68(5): 3534-3543.

[27] Ji R N, Song K, Guo X Y, et al. Spin-decoupled metasurface for broadband and pixel-saving polarization rotation and wavefront control[J]. Optics Express, 2021, 29(16): 25720-25730.

[28] Li S Q, Li X Y, Wang G X, et al. Multidimensional manipulation of photonic spin Hall effect with a single-layer dielectric metasurface[J]. Advanced Optical Materials, 2019, 7(5): 1801365.

[29] Huo P C, Zhang C, Zhu W Q, et al. Photonic spin-multiplexing metasurface for switchable spiral phase contrast imaging[J]. Nano Letters, 2020, 20(4): 2791-2798.

[30] Fu X M, Yang J, Wang J F, et al. Completely spin-decoupled geometric phase of a metasurface[J]. Photonics Research, 2023, 11(7): 1162-1174.

[31] Liu F, Wang D, Zhu H, et al. High-efficiency metasurface-based surface-plasmon lenses[J]. Laser & Photonics Reviews, 2023, 17(7): 2201001.

[32] Lin H, Lin Y C, Xiao L H, et al. Narrow-band rejection filter

based on spoof surface plasmons polariton[J]. Optical and Quantum Electronics, 2023, 55(5): 428-436.
[33] Wang Z, Li S Q, Zhang X Q, et al. Excite spoof surface plasmons with tailored wavefronts using high-efficiency terahertz metasurfaces[J]. Advanced Science, 2020, 7(19): 2000982.
[34] Wang X L, Zhao J H, Bo F, et al. Tightly focusing terahertz wave using gradient-type slotted grating based on spoof surface plasmons[J]. Optics Express, 2020, 28(11): 16298-16308.
[35] 胡凯, 葛益娴, 孙萌萌, 等. 基于多模-细芯-多模光纤结构的双参数测量传感器[J]. 激光与光电子学进展, 2023, 60(19): 1928002.
Hu K, Ge Y X, Sun M M, et al. Dual-parameter measurement sensor based on multi-mode-thin-core-multi-mode fiber structure[J]. Laser & Optoelectronics Progress, 2023, 60(19): 1928002.
[36] 朱华利, 张勇, 黎雨坤, 等. 基于InP工艺的小型化亚太赫兹人工表面等离子体激元传输线设计[J]. 光学学报, 2022, 42(21): 2124001.
Zhu H L, Zhang Y, Li Y K, et al. Design of compact sub-terahertz spoof surface plasmon polariton transmission line based on InP technology[J]. Acta Optica Sinica, 2022, 42(21): 2124001.
[37] 乔蔚, 胡梦云, 葛锦蔓, 等. 多光丝耦合诱导击穿光谱土壤微量元素检测[J]. 中国激光, 2023, 50(7): 0708009.
Qiao Y, Hu M Y, Ge J M, et al. Multi-filament interaction induced breakdown spectroscopy for trace element detection in soil[J]. Chinese Journal of Lasers, 2023, 50(7): 0708009.
[38] Mollet O, Huant S, Drezet A. Scanning plasmonic microscopy by image reconstruction from the Fourier space[J]. Optics Express, 2012, 20(27): 28923-28928.
[39] Khodadadi M, Moshiri S M M, Nozhat N, et al. Controllable hybrid plasmonic integrated circuit[J]. Scientific Reports, 2023, 13: 9983.
[40] Luo J, Wu Q L, Zhou L, et al. Plasmon-induced hot carrier dynamics and utilization[J]. Photonics Insights, 2023, 2(4): R08.
[41] Liu J F, Wu J W, Fu X J, et al. Spin-controlled reconfigurable excitations of spoof surface plasmon polaritons by a compact structure[J]. Laser & Photonics Reviews, 2023, 17(1): 2200257.
[42] Lin J, Mueller J P, Wang Q, et al. Polarization-controlled tunable directional coupling of surface plasmon polaritons[J]. Science, 2013, 340(6130): 331-334.
[43] Xu Z X, Tong J Y, Cui T J, et al. Near-field chiral excitation of universal spin-momentum locking transport of edge waves in microwave metamaterials[J]. Advanced Photonics, 2022, 4(4): 046004.
[44] Huang L L, Chen X Z, Bai B F, et al. Helicity dependent directional surface plasmon polariton excitation using a metasurface with interfacial phase discontinuity[J]. Light: Science & Applications, 2013, 2(3): e70.
[45] Sun S L, He Q, Xiao S Y, et al. Gradient-index meta-surfaces as a bridge linking propagating waves and surface waves[J]. Nature Materials, 2012, 11(5): 426-431.

Engineering Bi-Functional Wavefronts of Spoof Surface Plasmon Polaritons via Photonic Spin Decoupling

Yang Qingxiu[1], Xi Kelei[1], Zhou Shaodong[1], Sheng Xiaohang[1], Zhang Wenya[1,2], Gao Jingxiang[1], Wang Guifang[3], Zhuang Songlin[1], Cheng Qingqing[1,3*]

[1]*School of Optical-Electrical and Computer Engineering, University of Shanghai for Science and Technology, Shanghai* 200093, *China*;

[2]*Laboratory of Micro-Nano Optoelectronic Materials and Devices, Shanghai Institute of Optics and Fine Mechanics, Chinese Academy of Sciences, Shanghai* 201800, *China*;

[3]*Department of Respiratory Diseases and Critical Medicine, Quzhou Hospital Affiliated to Wenzhou Medical University, Quzhou* 324000, *Zhejiang*, *China*

Abstract

Objective In the realm of nanophotonics, the discovery of a geometric phase solely dependent on the rotation angle of metasurfaces has catalyzed a flurry of research activity. The breakthrough has facilitated the development of avant-garde scientific and technological applications, such as metasurface microscopy and compact spectrometers. However, a pivotal challenge lies in the inherent conjugate relationship between the geometric phases of different chiral circularly polarized lights. The relationship manifests as phase values that are equal in magnitude but opposite in sign, thus precluding independent and unrestricted manipulation of phase profiles for each chiral polarization state. Addressing the limitation requires transcending traditional paradigms of geometric phase control. Recent advancements propose a suite of innovative control methodologies, integrating phase mechanisms that are independent of structural rotation. These include the resonance phase, transmission phase, and roundabout phase. The paradigm shift paves the way for a burgeoning research field focusing on multi-degree-of-freedom light field control. Our core aspiration is to achieve independent phase control for each circularly polarized light and ensure efficient coupling of these controlled light fields with on-chip photonic structures. By tackling these challenges, we aim to unlock new dimensions in light manipulation at the nanoscale, potentially revolutionizing applications in optical computing, advanced imaging, and beyond.

Methods Based on the Jones matrix of the unit structure, our analysis elucidates the phenomenon of spin locking in the photonic Berry (PB) phase. This is attributed to the conjugate relationship between the PB phases carried by cross-polarized circularly polarized light, which is pivotal in manipulating light phase properties at the nanoscale. A key factor in the efficient coupling of the on-chip light field is the unique behavior of polarization coefficients. Specifically, we observe that the cross-polarization coefficient is effectively zero, while the co-polarization coefficient exhibits an inverse sign. These properties are instrumental in directing the light field's behavior. Furthermore, our metasurface design leverages the phase gradient at the interface to match the wave vector of surface plasmons. The approach facilitates efficient coupling of the on-chip light field, a critical factor in advanced photonic applications. Meanwhile, we introduce a novel strategy to break the PB phase conjugation relationship inherent in cross-polarized circularly polarized light. By integrating a chirality-independent resonance phase with the PB phase, we can exert distinct phase controls over the two circularly polarized lights. The innovation marks a significant advancement in phase manipulation techniques. Additionally, our structural design adheres to the mirror symmetry principles, which ensures that the cross-polarization coefficient remains zero, an essential condition for our intended phase control. By meticulously selecting parameters from our structure library, we tailor the co-polarization coefficients to differ by a π phase. The precision engineering is the key to yielding our desired light manipulation outcomes at the nanoscale.

Results and Discussions We report a significant advancement in the efficient coupling of on-chip light fields. Our approach enables the propagation mode of electromagnetic waves, which typically traverse in free space, to couple with on-chip surface plasmons. The coupling is achieved with remarkable efficiency, reaching up to 80% within 60 to 100 GHz frequency band. The high efficiency represents a noteworthy result in on-chip photonic systems, potentially paving the way for more compact and efficient photonic devices. Furthermore, our findings include groundbreaking development in the PB phase manipulation. We have successfully "unlocked" the spin of the PB phase, a significant stride in light manipulation at the nanoscale which allows for the directional propagation of left-hand and right-hand spins. Notably, they propagate to the left and right sides of the coupling structure respectively. The left-hand spins culminate as a Bessel beam channeling 37% of the energy, while the right-hand spins form a focused beam carrying 41% of the energy.

Conclusions We present a novel coupler design that capitalizes on the dual degrees of freedom offered by the resonance phase and the geometric phase. A key innovation of our design is the precise setting of the turning and opening angles of each unit cell. The meticulous configuration tackles a fundamental challenge in wavefront shaping, or the issue of varying circular shapes due to the geometric phase in dealing with circularly polarized light of different chiralities. Our approach effectively overcomes the limitations imposed by the conjugate phase under polarized light excitation. The advancement enables the wavefronts at both ends of the spectrum to be shaped independently, allowing for unprecedented control between different chiral incident polarized lights. By leveraging the methodology, we have successfully designed a dual-function wavefront-controlled coupler. The device exhibits remarkable capabilities in simultaneously focusing and generating Bessel beams. The multifunctionality is a significant stride forward in the wavefront manipulation field. Additionally, the developed coupling device is characterized by compact size and multifunctional nature. These attributes make it a promising candidate for functional design in integrated photonic integration. Finally, our study not only puts forward a practical solution to a complex challenge in photonics but also opens new avenues for the advancement of integrated photonic devices. The broad potential applications of the technology range from optical computing to advanced imaging systems, heralding a new era in integrated photonics.

Key words photonic spin Hall effect; polarization conversion; metasurface; high-efficiency coupler; surface wave